Re-evaluating stoichiometric estimates of iron valence in magmatic clinopyroxene crystals

David A. Neave*, Alexander G. Stewart, Margaret E. Hartley, Catherine McCammon

*david.neave@manchester.ac.uk

This is a non-peer reviewed preprint of an article resubmitted for publication in Contributions to Mineralogy and Petrology and uploaded to EarthArXiv in November 2023.

Re-evaluating stoichiometric estimates of iron valence in magmatic clinopyroxene crystals

David A. Neave[1*], Alexander G. Stewart[1], Margaret E. Hartley[1], Catherine McCammon[2]

[1*]Department of Earth and Environmental Sciences, The University of Manchester, Manchester, M13 9PL, United Kingdom.
[2]Bayerisches Geoinstitut, Universität Bayreuth, 95440 Bayreuth, Germany.

*Corresponding author(s). E-mail(s): david.neave@manchester.ac.uk;

Abstract

Clinopyroxene is a major rock forming mineral capable of incorporating diverse metal cations. As a consequence, clinopyroxene preserves valuable archives of magmatic processes. Understanding clinopyroxene is thus essential for understanding Earth's wider chemical evolution. However, knowledge about the relative abundances of ferrous and ferric iron in magmatic clinopyroxene remains sparse because it is not currently possible to routinely measure the valence of iron in clinopyroxene crystals without either separating single crystals for bulk analysis or securing access to Mössbauer spectroscopy or a synchrotron radiation source to perform *in-situ* microanalysis. This is despite magmatic clinopyroxene often containing appreciable quantities of ferric iron that will affect its stability and behaviour in currently ill-constrained ways and limit our ability to exploit its chemistry to robustly reconstruct the conditions of magma storage and evolution. Here we integrate optimised electron probe microanalysis and Mössbauer spectroscopy on endmember and single-crystal clinopyroxene samples to re-evaluate previously discredited approaches for estimating clinopyroxene ferric iron contents by stoichiometry. By ensuring that all major and minor elements in clinopyroxene crystals are measured with sufficient precision, we show that it is possible to readily obtain stoichiometric estimates of clinopyroxene ferric to total iron contents with similar precisions to those derived from Mössbauer spectroscopy ($1\boldsymbol{\sigma} \sim 3.5\%$ absolute). Being able to robustly determine clinopyroxene ferric iron contexts enables us to propose a new empirical scheme for assigning clinopyroxene components that explicitly accounts for ferric iron, which is primarily hosted within esseneite component ($CaFe^{\mathbf{3+}}AlSiO_{\mathbf{6}}$) in clinopyroxenes dominated by quadrilateral components and aegirine component ($NaFe^{\mathbf{3+}}Si_{\mathbf{2}}O_{\mathbf{6}}$)

in alkali clinopyroxenes. Our new scheme provides a framework for documenting the full spectrum of clinopyroxene compositions in studies on both natural and experimental systems when analyses have been performed with sufficient precision.

Keywords: clinopyroxene, ferric iron, stoichiometry, Mössbauer spectroscopy

1 Introduction

Clinopyroxene is a major constituent of diverse upper mantle and crustal rocks across all tectonic settings. This geologically significant mineral has the general formula $M2(R^{2+})M1(R^{2+})T_2(2R^{4+})O_6$, where R is a metal cation, M2 is a distorted octahedral site, M1 is a regular octahedral site and T is a tetrahedral site typically occupied by Si forming the Si_2O_6 chains that define the pyroxene structure (Morimoto et al, 1988). This variety of sites enables clinopyroxene to incorporate most of the major metal cations that occur in terrestrial magmas, making it a particularly valuable tool for reconstructing the thermochemical evolution of magmatic systems in space and time (e.g., Putirka et al, 1996; Wood and Blundy, 1997; Mollo et al, 2010; Petrone et al, 2016; Ubide and Kamber, 2018). However, the compositional complexity that results from this mineralogical plasticity also makes it challenging to model clinopyroxene phase equilibria (e.g., Sack and Ghiorso, 1994a; Green et al, 2007) and unambiguously disentangle the conditions and processes recoded by crystal compositions in both natural and experimental systems (e.g., Mollo et al, 2013; Neave et al, 2019; Ubide et al, 2019). Although understanding the chemistry of clinopyroxene is vital for understanding the chemical evolution of planetary interiors, much about this abundant and useful mineral remains poorly understood. For example, knowledge about the relative abundances of ferrous and ferric iron (Fe^{2+} and Fe^{3+}, respectively) in magmatic clinopyroxene, as well as their respective partitioning behaviours, is especially sparse. This is despite the ability of clinopyroxene to incorporate both Fe^{2+} and Fe^{3+} and potentially record information about magmatic oxygen fugacity (f_{O_2}) via its reactions with other phases, vital information for studying redox-dependent processes including such as evolution, ore mineralisation and volcanic degassing (Frost, 1991).

Oceanic basalts (mafic igneous rocks erupted at mid-ocean ridges and ocean islands), which dominate Earth's magma budget, frequently contain significant quantities of augitic clinopyroxene. Augite has the general formula $Ca(Mg,Fe^{2+})Si_2O_6$ and is the mineral name given to the solid solution between Mg-rich diopside (Di; $CaMgSi_2O_6$) and Fe^{2+}-rich hedenbergite (Hd; $CaFe^{2+}Si_2O_6$; Deer et al, 2013). Augite, diopside and hedenbergite have standard site occupancies, with Ca^{2+} on their M2 sites, Mg^{2+} and Fe^{2+} (and minor Mn^{2+}) on their M1 sites and tetravalent Si^{4+} on their T sites. However, pure augite is rare in nature, with most natural crystals incorporating small amounts of Ca-poor enstatite (En; $Mg_2Si_2O_6$) and ferrosilite (Fs; $Fe_2^{2+}Si_2O_6$) components alongside various others. One of the most prevalent substitutions responsible for the incorporation of other components involves the coupled substitution of R^{2+} on the M1 site and R^{4+} on a T site with R^{3+} on both the M1 site and a T site.

For example, $(Mg,Fe)^{2+}$ and Si^{4+} are commonly replaced with Al^{3+} to create calcium Tschermak's component (CaTs; $CaAlAlSiO_6$). Indeed, that the Al_2O_3 content of clinopyroxene crystals from oceanic basalts ranges from ∼2 wt.% in tholeiitic mid-ocean-ridge and Icelandic basalts (e.g., Bryan et al, 1981; Jakobsson et al, 1978) to >10 wt.% in alkaline basanites and ankaramites from the Canary Islands and Hawaii (e.g., Klügel et al, 2005; Hammer et al, 2016) attests to the importance of Al-rich components in natural clinopyroxene crystals. The componentry scheme of Putirka et al (2003) also incorporates Cr^{3+}, which occurs at levels up to 2 wt.% Cr_2O_3 in some primitive augite crystals (Maclennan et al, 2003), via a similar substitution to form chromium calcium Tschermak's component (CrCaTs; $CaCrCrSiO_6$).

The substitution of R^{2+} on both the M2 and M1 sites with R^{1+} on the M2 site and R^{3+} on the M1 site is of particular significance because the formation of Na^{1+}- and Al^{3+}-bearing jadeite component (Jd; $NaAlSi_2O_6$) depends strongly on pressure and can therefore be exploited as a geobarometer (Blundy et al, 1995; Putirka et al, 1996). Specifically, the large partial molar volume change associated with Jd formation means that clinopyroxene formed at high pressures contain more Jd than that formed from similar melts at low pressures, a phenomenon that has been exploited in the calibration of diverse clinopyroxene-based geobarometers (e.g., Putirka et al, 1996; Putirka, 2008; Neave and Putirka, 2017; Wang et al, 2021). Another important and analogous substitution concerns the formation of Na^{1+}- and Fe^{3+}-bearing aegirine component (Ae; $NaFe^{3+}Si_2O_6$). Clinopyroxene crystals dominated by Ae, referred to by the mineral name aegirine, are found in highly evolved alkaline rocks like those from the Ilímaussaq intrusion in Greenland (e.g., Larsen, 1976), though Ae-rich augite (aegirine-augite) also occurs in less extreme alkaline differentiates like those found on Pantelleria, Italy (e.g., White et al, 2005). However, the importance of Ae component in clinopyroxene crystals from oceanic basalts remains unclear, partly because they contain little Na but also because of uncertainties in how much Fe^{3+} they contain and the mechanisms by which this Fe^{3+} is incorporated.

Augite contains significant amounts of Fe, which is typically reported with the assumption that that all Fe occurs as Fe^{2+} (i.e., FeO_T) because it is impossible to determine Fe valence from routine Fe$K\alpha$ emission spectroscopy by electron probe microanalysis (EPMA). Measuring Fe$L\alpha$ and Fe$L\beta$ emission lines can provide information about Fe valence but remains to be demonstrated conclusively for clinopyroxene (Smith and O'Nions, 1971; Höfer et al, 1994; Höfer and Brey, 2007). Nonetheless, the few direct determinations of Fe valence in magmatic clinopyroxene crystals available from Mössbauer spectroscopy suggest that ratios of Fe^{3+} to total Fe (i.e., $Fe^{3+}/\Sigma Fe$) are well above zero in many cases and can reach up to 0.6 in crystals from mafic alkaline rocks erupted in the Canary Islands and elsewhere (McGuire et al, 1989; Weis et al, 2015), in line with legacy wet chemical datasets (e.g., Deer et al, 2013). This variability in clinopyroxene $Fe^{3+}/\Sigma Fe$ is perhaps unsurprising given that glass $Fe^{3+}/\Sigma Fe$ contents spanning the range ∼0.14–0.35 have now been documented by Fe X-ray absorption near edge structure (Fe-XANES) spectroscopy on oceanic basalt glasses (Shorttle et al, 2015; Moussallam et al, 2016; Brounce et al, 2017; Zhang et al, 2018; Moussallam et al, 2019). Overall, these observations imply that Fe^{3+} is a cryptic but significant

constituent of clinopyroxene crystals from oceanic basalts. The relatively low Na content of most magmatic augite crystals (usually <1 wt.% Na_2O; Wieser et al, 2023) precludes the significant incorporation of Fe^{3+} as an Ae component because there is insufficient Na^{1+} to balance all of the Fe^{3+} present. Comparisons with mantle clinopyroxenes and the apparent insensitivity of Jd formation to f_{O_2} hence suggest that Fe^{3+} could be incorporated as esseneite component (Es; $CaFe^{3+}AlSiO_6$) via a Tschermak-type substitution (Luth and Canil, 1993; Neave et al, 2019). However, the systematic determinations of $Fe^{3+}/\Sigma Fe$ in magmatic clinopyroxenes needed to substantiate this suggestion remain elusive.

Mössbauer spectroscopy provides an accurate and precise way of determining clinopyroxene $Fe^{3+}/\Sigma Fe$ (e.g., McGuire et al, 1989; Canil and O'Neill, 1996; Sobolev et al, 1999). However, few labs have the necessary equipment and capacity to process large numbers of samples. Moreover, analytical spot sizes typically exceed 100 μm (McCammon, 1994), making the technique of limited use for studying magmatic crystals. Synchrotron Mössbauer spectroscopy offers exciting opportunities for working on small samples (spot sizes ≤50 μm) but is relatively challenging to access given the limited number of facilities available globally (McCammon, 2021). Crystal anisotropy also makes it challenging to use synchrotron-based Fe-XANES spectroscopy to determine clinopyroxene $Fe^{3+}/\Sigma Fe$, though this approach certainly warrants continued exploration thanks to its theoretically high precision (Dyar et al, 2002; McCanta et al, 2004; Steven et al, 2022). Applying stoichiometric criteria to EPMA data provides an alternative and relatively accessible way to estimate $Fe^{3+}/\Sigma Fe$. One approach proposed by Papike (1974) and further popularised by Lindsley (1983) balances Na^{1+} on the M2 site and Al^{3+} on T sites with Al^{3+}, Cr^{3+}, Fe^{3+} and Ti^{4+} on the M1 site ($Na + Al^{IV} = Al^{VI} + Cr + Fe^{3+} + 2Ti^{4+}$). A more general approach proposed Droop (1987) estimates the amount of Fe^{3+} from the excess cations remaining after calculating clinopyroxene formulae on a six-oxygen basis. Specifically, Droop (1987) suggests that the amount of Fe^{3+} per X oxygen anions (where $X = 6$ for clinopyroxene), F, is given by:

$$F = 2X(1 - T/S), \tag{1}$$

where T is the ideal number of cations (where $T = 4$ for clinopyroxene), and S is the observed cation total per X oxygens when all Fe is assumed to be Fe^{2+}. Unfortunately, considerable doubt surrounds using stoichiometry to determine clinopyroxene $Fe^{3+}/\Sigma Fe$, with McGuire et al (1989) suggesting that it may be associated with absolute uncertainties of 25%, rendering the approach essentially useless for addressing geological problems, a conclusion reinforced by the sensitivity assessment performed by Canil and O'Neill (1996). However, recent re-evaluations of uncertainties in clinopyroxene compositions determined by EPMA suggest that the precision of many elements, including minor elements like Na, Cr and Mn that are of particular relevance for performing precise geothermobarometry, may be relatively poor (Wieser et al, 2023). Poor analytical precision may have thus confounded past attempts to estimate clinopyroxene $Fe^{3+}/\Sigma Fe$ by stoichiometry, an approach that ultimately depends on the accurate

and precise calculation of cation sums. We aim to critically re-evaluate the viability of using stoichiometry as an accessible approach for determining clinopyroxene $Fe^{3+}/\Sigma Fe$.

Clinopyroxene compositions reported as element oxides are often recast into endmember components that notionally reflect the incorporation of diverse clinopyroxene components (real and fictive) via multiple solid solutions (e.g., Di–Hd and DiHd–Jd) into a single solid phase. As well as providing a convenient way to summarise clinopyroxene compositions, these components often serve endmembers in both empirical and thermodynamic models used to address geological problems (Lindsley, 1983; Sack and Ghiorso, 1994a; Putirka et al, 1996; Holland and Powell, 1998; Jennings and Holland, 2015). This is because mineral-melt and mineral-mineral reactions often take place between a subset of components. For example, Fe^{2+}–Mg exchange between clinopyroxene and melt will only directly affect Mg and Fe^{2+} bearing quadrilateral components (Di, Hd, En and Fs directly); effects on non-quadrialteral components (like Jd or CaTs) will be indirect. However, most schemes currently available for assigning clinopyroxene components either make now discredited assumptions about the components present or fail to account for the full range of elements present in natural crystals, limiting their usefulness. In particular, the widely used scheme described by Putirka et al (1996) and modified Putirka et al (2003) does not account for the presence of Fe^{3+}, while the scheme described by Lindsley (1983) assumes that all Fe^{3+} is balanced by Na in Ae and does not consider Ti despite its prevalence in many augite crystals (Leung, 1974). We aim to provide a new scheme for assigning clinopyroxene components that provides a more holistic reflection of clinopyroxene compositions that will support future work.

Here we present high-precision EPMA analyses of endmember and single-crystal clinopyroxene samples on which we have also performed Mössbauer spectroscopy in order to critically re-evaluate the utility of determining clinopyroxene $Fe^{3+}/\Sigma Fe$ by stoichiometry. Having established that stoichiometry can indeed provide robust estimates of clinopyroxene $Fe^{3+}/\Sigma Fe$ we use our analyses to propose a revised scheme for assigning clinopyroxene components that explicitly accounts for all cations present including Fe^{3+}. This scheme will allow enable more robust comparisons of clinopyroxene compositions across diverse natural and experimental samples.

2 Samples

We collected seven endmember and single-crystal clinopyroxene samples from mineral collections at Manchester Museum (MM) and the Department of Earth and Environment Sciences (DEES) at The University of Manchester to span a wide range of clinopyroxene compositions (Table 1). Specifically, we collected two aegirine crystals from evolved alkaline igneous rocks, two augite crystals from mafic alkaline rocks, one diopside crystal, one block of intergrown hedenbergite crystals from a skarn and one sample of intergrown clinopyroxene crystals of unclear affinity (labelled as diopside but described below as 'other'). Single crystals were cut into at least four pieces, with three pieces being roughly oriented and mounted in epoxy for microanalysis (including Fe-XANES spectroscopy to be described in a subsequent manuscript) and one piece being powdered under isopropanol in an agate mortar for Mössbauer spectroscopy; pieces

adjacent to the powdered piece were filtered for inclusions and chemical heterogeneities using the microscopy methods described below prior to performing Mössbauer spectroscopy. Powders were then sandwiched between cellophane in ∼0.5 mm diameter holes drilled through 0.5 mm-thick wafers of Pb foil. Multiple wafers were prepared for samples containing low total Fe contents. One important exception concerns the piece of augite 2 used for Mössbauer spectroscopy that was mechanically separated from an oxide-free part of a otherwise Fe-Ti oxide-rich crystal identified from microscopy (see below). Intergrown samples of hedenbergite and the other clinopyroxene were also mounted in epoxy for microanalysis after mechanically removing chips to powder for Mössbauer spectroscopy. A 1" epoxy mount containing chips of the seven clinopyroxene samples is available for loan from the corresponding author on request.

3 Methods

3.1 Microscopy

Epoxy mounts of endmember and single-crystal clinopyroxene samples were investigated with a FEI Quanta 650F scanning electron microscope (SEM) in the Department of Earth and Environmental Sciences at The University of Manchester to characterise compositional variability within and between samples. Backscattered electron (BSE) imaging was performed identify targets for microanalysis that avoided inclusions and chemical heterogeneities. Imaging was also performed to confirm whether samples were suitable (i.e., sufficiently free from inclusions) for bulk analysis by Mössbauer spectroscopy or whether subsampling of specific crystal portions was required (representative BSE images are provided in Figure 1). Clinopyroxene compositions were also determined qualitatively by energy dispersive X-ray spectroscopy (EDS) using an Brucker Quantax system to ensure that the correct elements were selected for quantitative analysis by EPMA. Measuring all minor elements present in EDS spectra is vital for properly quantifying clinopyroxene compositions (Wieser et al, 2023).

3.2 Electron probe microanalysis

Quantitative analyses were performed by EPMA using a JEOL JXA8530F instrument in the School of Earth Sciences at the University of Bristol operated with Probe for EPMA (https://www.probesoftware.com/). The following primary standards were used for calibration: Si, albite; Ti, TiO_2; Al, sanidine; Cr, Cr_2O_3; Fe, hematite; Mn, Mn metal; Mg, St. John's Island olivine; Ca, wollastonite; Na, albite; K, sanidine; P, Durango apatite; and Ni, Ni metal.

Particular care was taken over the analysis of clinopyroxene to re-evaluate whether clinopyroxene $Fe^{3+}/\Sigma Fe$ can be determined precisely by stoichiometry. We used an accelerating voltage of 15 kV and a spot size of 1 μm. The following elements were analysed with a current of 10 nA (on-peak counting times in seconds are shown in parentheses; background counting times were half on-peak counting times on each side of the peak): Si(20), Ti(20), Al(20), Fe(40), Mg(40), Ca(20) and K(40); and the following elements were analysed with a current of 40 nA: Cr(60), Mn(30), Na(60), P(60) and Ni(30). We used this approach to maximise the precision of minor element analyses

while minimising the risk of sample damage during major element analysis. Optimising minor element analyses is important because the quality of minor element data fundamentally affects the precision of thermobarometric calculations (Wieser et al, 2023), and is thus likely to affect the precision of clinopyroxene $Fe^{3+}/\Sigma Fe$ determinations by stoichiometry in a similar way. We suggest that a realistic aim when measuring clinopyroxene by EPMA is to analyse each element at a sufficient current and for a sufficiently long time to return 1σ precisions from counting statistics on the order of 2% or better for major elements and 5% or better for minor elements. Importantly, monitoring the time-dependent intensity of Na counts has demonstrated that Na remains immobile when analysing augitic clinopyroxene crystals with a focused beam at 40 nA or even 100 nA (Wieser et al, 2023). Nonetheless, we recommend verifying that unknowns are stable under the beam conditions in question prior to analysis.

Accuracy was monitored by analysing the following secondary standards: an in-house diopside, an in-house Cr-diopside, MongOl olivine (Batanova et al, 2017) and kk1 kaersutite (Reay et al, 1989). Major element (e.g., SiO_2 and MgO) concentrations were typically within 2% of preferred values (based on published values or longitudinal data for in-house standards), while minor element (e.g., Cr_2O_3 and Na_2O in Cr-diopside) concentrations were typically within 6% of preferred values. However, validating the accuracy of minor element analyses with international clinopyroxene standards is challenging because of lingering uncertainties about standard homogeneity (Fournelle and Scott, 2017). While no standard is perfect, we suggest that the Cr-augite (NMNH 164905) described by Jarosewich et al (1987) is probably the best widely available material for validating EPMA accuracy when seeking to determine clinopyroxene $Fe^{3+}/\Sigma Fe$; we aim to validate the suitability of NMNH 164905 as part of ongoing research because we were unable to analyse it during the EPMA sessions that supported this work. Counting statistics from analyses of unknown clinopyroxene crystals indicate that major (SiO_2, Al_2O_3, FeO_T, MgO and CaO) and minor (TiO_2, Cr_2O_3 and Na_2O) elements were measured with 1σ precisions better than 1% and 5%, respectively; only MnO was measured with a worse 1σ precision of ∼8%. Full details of secondary standard analyses and analytical precision are provided in the Supplementary Material alongside all EPMA data.

3.3 Mössbauer spectroscopy

Mössbauer spectroscopy was performed on powdered endmember and single-crystal clinopyroxene samples sandwiched between cellophane in ∼0.5 mm diameter holes drilled through 0.5 mm-thick wafers of Pb foil. Multiple wafers were prepared for samples with low FeO_T contents (<5 wt.%) to ensure that effective sample thicknesses were sufficient for high quality analysis (McCammon, 2021). Spectra were collected using a constant acceleration Mössbauer spectrometer with a nominal 450 MBq ^{57}Co high specific activity source in a 12 μm-thick Rh matrix in the Bayerisches Geoinstitut at the Universität Bayreuth. Velocity scales were calibrated against a 25 μm-thick α-Fe foil using positions from standard reference material 1541 of the (former) National Bureau of Standards. Outer line widths of 0.36 mm/s were obtained for α-Fe at room temperature. Spectra were fitted with the MossA programme using the full transmission

integral as described by Prescher et al (2012). Fits are illustrated in Supplementary Figures 1 and 2 and hyperfine parameters are provided in the Supplementary Material.

Fits were optimised to accurately determine relative areas for total Fe^{2+} and Fe^{3+}. We used variable numbers of pseudo-Voigt doublets depending on the complexity of the spectra without consideration for crystal structure. Augite spectra could be well fitted using one doublet for Fe^{2+} and one for Fe^{3+}, while all other spectra required an additional Fe^{2+} doublet. The aegirine 2 spectrum required an additional singlet for Fe^{3+}. It is likely that the need for both a doublet and a singlet to fit Fe^{3+} simply indicates variation in the atomic environment due to different next-nearest neighbour configurations rather than different crystallographic sites. The quality of fits to Mössbauer spectra indicates that 1σ analytical uncertainties in $Fe^{3+}/\Sigma Fe$ determinations are 0.02–0.03 absolute for all samples except the other clinopyroxene, which was subject to a slightly larger absolute uncertainty of 0.05 because of its low FeO_T content and compositional heterogeneity (see below).

4 Results

4.1 Clinopyroxene textures

Backscattered electron images of characteristic textures in endmember and single-crystal clinopyroxene samples are shown in Figure 1. Neither aegirine 1 nor aegirine 2 show clear evidence for internal compositional zoning, though the former hosts fractures with low volumes of both low- and high-BSE-intensity phases, and the latter contains diffuse bands of small crystals with high BSE intensities (Figures 1A and B, respectively). While too small to measure by EPMA, EDS analyses suggest that the high-BSE-intensity phases are Fe-Ti oxides. While such oxides could compromise bulk $Fe^{3+}/\Sigma Fe$ determinations, they make up much less that 1 vol.% of the crystals and would therefore exert little leverage over the resulting Mössbauer spectra, especially given the high FeO_T of the aegirine samples in question. Most pieces of augite 1 show no evidence for compositional zoning (Figure 1C), though some show minor core-rim zoning (Supplementary Figure 3); inclusions of Fe-Ti oxide are sufficiently sparse to have minimal effect on Mössbauer spectra. Despite showing no evidence for compositional zoning, augite 2 contains abundant and large Fe-Ti oxide inclusions (Figure 1D). However, material for Mössbauer spectroscopy was mechanically sampled from an inclusion-poor portion of the crystal, alleviating the risk of contamination. The diopside is homogeneous and inclusion-free (Figure 1E), while the other clinopyroxene is inclusion free but compositionally zoned in complex ways that could not be mitigated against during sampling for Mössbauer spectroscopy (Figure 1F). The hedenbergite sample contains fibrously intergrown but compositionally homogeneous crystals (Supplementary Figure 4).

4.2 Major element chemistry

The major element chemistry of endmember and single-crystal clinopyroxene samples is summarised in Figure 2, Table 2 and Table 3. The Q–J diagram in Figure 2A demonstrates that all our endmember and single-crystal clinopyroxene samples, with

the exception of the two Na-rich aegirine samples, are dominated by quadrilateral components (Morimoto et al, 1988). Again with the exception of the two aegirine samples, all of our samples fall along the Di-Hd tie line on a pyroxene quadrilateral calculated assuming that the Fe component (ΣFe*) is equal to the sum of Fe^{2+}, Fe^{3+} and Mn (Figure 2B; Morimoto et al, 1988). The diopside and other clinopyroxene fall close to the Di apex, the hedenberite falls close to the Hd apex, and, as expected, the aegirine samples fall close to the Fs apex by virtue of their high total Fe contents but low Ca contents. The two augite samples fall between the the Di and Hd apices and contain very little En or Fs components.

Endmember and single-crystal clinopyroxene sample Na_2O contents are summarised in Figure 3A. Excluding the aegirine samples, which contain ∼12–13 wt.% Na_2O, our clinopyroxene samples contain 0.1–0.5 wt.% Na_2O, with the augite samples being relatively enriched in Na when compared with the diopside and hedenbergite. Almost all endmember and single-crystal clinopyroxene samples contain very little Cr_2O_3, with only the diopside and augite 1 (and one piece of augite 3) containing appreciable but variable Cr_2O_3 contents indicative of internal zoning (Figure 3B). Variations in sample Ti and Al contents are shown in Figure 3C. Only the augite samples contain meaningful concentrations of both Al and Ti that fall along lines of constant Ti:Al. Both aegirine crystals contain significant but variable amounts of Ti.

4.3 Iron contents and valence systematics

The FeO_T content of endmember and single-crystal clinopyroxene samples is summarised in Figure 4A, and ranges from ∼1–3 wt.% in the diopside and other clinopyroxene through ∼7 wt.% in the augite samples to ∼26–29 wt.% in the aegirine samples and hedenbergite. Although analytical uncertainty is the main control over FeO_T variability in some clinopyroxene samples (augite 2, aegirine 2 and hedenbergite), other samples show variability consistent with intra-mineral compositional zoning (augite 1, aegirine 1 and the other clinopyroxene), which is visible in BSE images of some crystals (e.g., Fig 1F).

Endmember and single crystal clinopyroxene sample $Fe^{3+}/\Sigma Fe$ contents determined by Mössbauer spectroscopy are summarised as a function of FeO_T in Figure 4B and are provided in Tables 2 and 3. Although multiple pieces of these clinopyroxene samples (n = 2–5) were analysed multiple times by EPMA to produce the piece-wise mean compositions plotted in Figure 4B and sample-wise mean concentrations collated in Tables 2 and 3 (n = 3–10 per piece and n = 12–36 per sample), only one Mössbauer spectrum was collected per sample. Uncertainties in $Fe^{3+}/\Sigma Fe$ do not vary strongly with FeO_T or $Fe^{3+}/\Sigma Fe$. As anticipated, the diopside and hedenbergite contain barely detectable amounts of Fe^{3+} ($Fe^{3+}/\Sigma Fe$ of 0.03±0.02(1σ) and 0.05±0.02(1σ), respectively). Conversely, the two aegirine samples are dominated by Fe^{3+} but still contain appreciable Fe^{2+} ($Fe^{3+}/\Sigma Fe$ contents of 0.84±0.03(1σ) and 0.93±0.03(1σ) in aegirine 1 and aegirine 2, respectively). Augites 1 and 2 contain intermediate $Fe^{3+}/\Sigma Fe$ contents of 0.56±0.03(1σ) and 0.42±0.03(1σ), respectively. The other clinopyroxene also has an intermediate $Fe^{3+}/\Sigma Fe$ value of 0.50±0.05(1σ) and could be considered as ferrian diopside (Morimoto et al, 1988).

5 Discussion

5.1 Re-evaluating stoichiometric estimates of iron valence

Clinopyroxene $Fe^{3+}/\Sigma Fe$ contents determined by Mössbauer spectroscopy are compared with $Fe^{3+}/\Sigma Fe$ contents determined by stoichiometry following Droop (1987) in Figure 5A. Uncertainties in $Fe^{3+}/\Sigma Fe$ contents from stoichiometry were determined for each clinopyroxene piece using a Monte Carlo approach. Specifically, oxide concentrations determined by EPMA were repeatedly resampled ($n = 100$) to distributions described by 1σ analytical uncertainties from counting statistics. This approach does not account for correlated uncertainties in EPMA data, nor does it fully propagate the analytical uncertainties on individual elements across all cations during normalisation calculations. It does, however, provide conservative (i.e., upper) and interenally consistent estimates of uncertainties and hence informs the robustness of $Fe^{3+}/\Sigma Fe$ determinations obtained when EPMA analyses are accurate within the tolerances described in the Methods. For instance, uncertainties in $Fe^{3+}/\Sigma Fe$ decrease with increasing FeO_T (Figure 6A), with the Fe-poor other clinopyroxene subject to considerably larger uncertainties than the rest of the sample suite. This trend results from the plateauing of 1σ uncertainties at ~0.35 wt.% Fe_2O_3 in our dual-condition setup optimised for high-precision clinopyroxene analyses (Figure 6B), a value that reflects the combined uncertainties in all elements analysed by EPMA rather than the uncertainty of FeO_T analyses alone, and will vary across different sessions and instruments. By comparison, estimating uncertainties using counting statistics from routine EPMA approaches such as those used by Neave et al (2019) that typically measure minor elements for 10 s at 10 nA rather than for 30–60 s at 40 nA return considerably larger 1σ uncertainties of ~0.85 wt.% Fe_2O_3.

Linear regression shows that clinopyroxene $Fe^{3+}/\Sigma Fe$ contents determined by stoichiometry following Droop (1987) correlate positively and strongly with $Fe^{3+}/\Sigma Fe$ contents determined by Mössbauer spectroscopy ($r^2 = 0.99$), with the mean 1σ prediction interval of the regression (0.035) being comparable to 1σ analytical uncertainties associated with Mössbauer spectroscopy (0.03–0.05) and similar in magnitude to uncertainties in minor element concentrations. Uncertainties in the $Fe^{3+}/\Sigma Fe$ content of augite samples estimated using the Monte-Carlo approach described above are comparable in magnitude to those estimated from the regression against results from Mössbauer spectroscopy and lie close to ~$0.05(1\sigma)$. Importantly, these uncertainties increase by a factor of three to ~$0.16(1\sigma)$ when performing equivalent calculations using counting statistics from the more routine EPMA approaches considered above, demonstrating the importance of optimising analytical conditions if seeking to determine $Fe^{3+}/\Sigma Fe$ by stoichiometry.

McGuire et al (1989) observed that the $Fe^{3+}/\Sigma Fe$ contents of (three) augite crystals determined by stoichiometry assuming four cations did not correlate with their $Fe^{3+}/\Sigma Fe$ contents determined by Mössbauer spectroscopy. Unfortunately, they do not provide detailed information about the precision of their EPMA analyses, only quoting relative uncertainties of 0.5–2% and 10–20% for major and minor elements, respectively, that were obtained by counting for 30 s at 20 nA. Illustrative calculations performed by applying conservative estimates of their uncertainties to our augite

data (1% relative on major elements present at >1 wt.% and 10% relative on minor elements present at <1 wt.%) revlealed larger uncertainties than those obtained with our optimised EPMA approach ($\sim$0.11(1σ) versus $\sim$0.05(1σ)). Indeed, uncertainties of this magnitude could account for the poor correspondence between stoichiometry and Mössbauer spectroscopy in their study. Moreover, McGuire et al (1989) note that stoichiometric calculations are highly sensitive to analytical accuracy, with the accuracy of relatively abundant SiO_2 being especially important. However, they also note that they found it challenging to determine SiO_2 with an accuracy better than 1 wt.%, (equivalent to $\sim$2% relative), a value impossible to verify in the absence of secondary standards being reported but nonetheless capable of imposing an additional error of 0.1 on estimated $Fe^{3+}/\Sigma Fe$ contents. Fortunately, though perhaps unsurprising given 30 intervening years of technique development, secondary standard analyses suggest that our data considerably more accurate than those of McGuire et al (1989), with our best constrained standards, MongOL (Batanova et al, 2017) and kk1 (Reay et al, 1989), indicating SiO_2 accuracies better than 0.5% relative (see Supplementary Material).

Canil and O'Neill (1996) suggested that uncertainties in stoichiometric estimates of clinopyroxene $Fe^{3+}/\Sigma Fe$ contents may reach up to $\sim$0.5(1σ), rendering them essentially useless for geological applications. However, repeating the Monte Carlo calculations described above using analytical uncertainties estimated from the expressions given in Table 4 of Canil and O'Neill (1996), who analysed samples for 20 s at 15 nA, returned much smaller estimates of $Fe^{3+}/\Sigma Fe$ uncertainty ($\sim$0.07(1σ)). The key reason for this difference in estimated uncertainties is that Canil and O'Neill (1996) estimated $Fe^{3+}/\Sigma Fe$ uncertainties using a statistical approach for determining the most probable stoichiometric formula rather than propagating analytical uncertainties through the Droop (1987) algorithm. We also note that Canil and O'Neill (1996) investigated mantle crystals with considerably less FeO_T than the magmatic crystals considered here ($\sim$3 wt.% versus >6 wt.%). They also do not present any analyses of secondary standards that could be used to verify the accuracy of their EPMA data used to estimate $Fe^{3+}/\Sigma Fe$. While Canil and O'Neill (1996) raise many important issues associated with determining $Fe^{3+}/\Sigma Fe$ by stoichiometry, we believe that their assessment was overly pessimistic when compared with the considerably more coherent results presented in Figure 5A.

Stoichiometric determinations performed following Papike (1974) are less successful for our clinopyroxene samples than those performed following Droop (1987): $r^2 = 0.92$ with a mean 1σ prediction interval of $\sim$0.104. In particular, estimated $Fe^{3+}/\Sigma Fe$ contents for the augite samples and other clinopyroxene are inaccurate and lie up to 0.2 below a one-to-one line despite estimated $Fe^{3+}/\Sigma Fe$ contents for the diopside, hedenbergite and aegirine samples falling on the one-to-one line (Figure 5B). Given that $Fe^{3+}/\Sigma Fe$ in magmatic clinopyroxene crystals ranges between 0 and 0.6 (McGuire et al, 1989; Weis et al, 2015) and that most magmatic clinopyroxene crystals are augitic in composition, applying the approach of Papike (1974) would result in the widespread underestimation of $Fe^{3+}/\Sigma Fe$ by 0.2, equivalent to relative inaccuracies of 33–100%. We suggest that the charge balance relationship proposed by Papike (1974), which only describes one mechanism for substituting Fe^{3+} into clinopyroxene ($Na + Al^{IV} = Al^{VI} + Cr + Fe^{3+} + 2Ti^{4+}$), provides an incomplete description of how Fe^{3+} is

incorporated into magmatic augite. In contrast the approach of Droop (1987), which considers all cations, can implicitly account for all mechanisms of Fe^{3+} incorporation as long as Fe is the only multivalent element present, a reasonable assumption for most terrestrial magmas. We therefore believe that clinopyroxene $Fe^{3+}/\Sigma Fe$ contents can be determined accurately and precisely using the approach of Droop (1987) when EPMA is carried out with sufficient care and analytical uncertainties are documented robustly.

5.2 Accounting for ferric iron in clinopyroxene componentry

The componentry scheme described by Putirka et al (1996) is widely used as the basis for empirical thermobarometers (e.g., Putirka, 2008; Neave and Putirka, 2017). This scheme forms Jd first, and also incorporates Ti via a titanium pyroxene component (CaTi; $CaTiAl_2O_6$) through $TiAl_2$–$MgSi_2$ exchange (Robinson, 1980; Sack and Carmichael, 1984). Despite the incorporation of Cr via chromium Tschermak's component (CrCaTs; $CaCr_2SiO_6$) in a later modifcation by Putirka et al (2003), this scheme still does not account for Fe^{3+}. This is at least partly because Putirka et al (1996) assumed that Fe^{3+} was absent from their graphite-buffered experiments. We also speculate that it reflects incoherence in clinopyroxene Fe^{3+} systematics estimated from legacy EPMA datasets using stoichiometric criteria, especially given the likely inaccuracy of values estimated following the approach of Papike (1974).

An alternative scheme described by Sack and Ghiorso (1994a,b) and implemented in the MELTS algorithm (e.g., Ghiorso and Sack, 1995) incorporates Ti via the fictive buffonite (Bf; $CaMg_{0.5}Ti_{0.5}Fe^{3+}SiO_6$) and alumino-buffonite (ABf; $CaMg_{0.5}Ti_{0.5}AlSiO_6$) components on the basis of miscibility gaps in the Di–CaTi–CaTs ternary and combined $TiAl_2$–$MgSi_2$, Al–Fe^{3+} and Al_2–MgSi exchanges observed in natural samples; ABf falls halfway between Di and CaTi, and Bf is related to ABf by Al–Fe^{3+} exchange. Ferric iron is also incorporated within Es via Al–Fe^{3+} exchange with CaTs. We note that Es serves as an major host of Fe^{3+} in the databases described by Jennings and Holland (2015) and Holland et al (2018) that underpin calculations performed with the THERMOCALC algorithm (e.g., Powell et al, 1998). However, we urge caution in using the MELTS algorithm to interpret clinopyroxene Fe^{3+} contents given that the models described by Sack and Ghiorso (1994a,b) were calibrated using stoichiometric estimates of $Fe^{3+}/\Sigma Fe$ obtained from EPMA performed under ill-defined conditions and with ill-defined uncertainties. Moreover the clinopyroxene database used for calibrating the MELTS algorithm is biased towards the products of experiments performed on highly alkaline compositions at atmospheric pressure under highly oxidising conditions that may not capture the behaviour of most magmatic clinopyroxene crystals. A new empirical scheme for assigning clinopyroxene components is therefore needed to provide a complete if empirical description of clinopyroxene compositions in light of our ability to reliably estimate clinopyroxene Fe^{3+} via optimised EPMA.

We propose that components in magmatic clinopyroxene crystals can be calculated using the following scheme based on that described by Putirka et al (1996):

1. Calculate clinopyroxene cation fractions (X_{cation}) from oxide concentrations on a six oxygen basis
2. Determine clinopyroxene $X_{Fe^{2+}}$ and $X_{Fe^{3+}}$ contents following Droop (1987), encompassing the renormalisation of cations (including total Fe) by multiplying each cation by T/S as outlined in his point (iv); the total number of all original cations will now equal four and values of $X_{Fe^{2+}}$ and $X_{Fe^{3+}}$ can be used to convert FeO_T into FeO and Fe_2O_3
3. Determine the relative proportions of tetrahedral and octahedral Al (Al^{IV} and Al^{VI}, respectively) such that $X_{Al^{IV}} = 2 - X_{Si}$ and $X_{Al^{VI}} = X_{Al} - X_{Al^{IV}}$; if X_{Si} exceeds 2 there is no $X_{Al^{IV}}$
4. Form Jd ($NaAlSi_2O_6$) from whichever is less between Na and Al^{VI} such that $X_{Jd} = X_{Na}$ or $X_{Jd} = X_{Al^{VI}}$
5. Form Ae ($NaFe^{3+}Si_2O_6$) from whichever is less between Na remaining after Jd formation and Fe^{3+} such that $X_{Ae} = X_{Na} - X_{Jd}$ or $X_{Ae} = X_{Fe^{3+}}$
6. Form neptunite (Np; $NaFe^{2+}_{0.5}Ti_{0.5}Si_2O_6$) from any Na remaining after Ae formation such that $X_{Np} = X_{Na} - X_{Jd} - X_{Ae}$; only relevant for alkali clinopyroxenes
7. Form Es ($CaFe^{3+}AlSiO_6$) from any Fe^{3+} remaining after Ae formation such that $X_{Es} = X_{Fe^{3+}} - X_{Ae}$
8. Form CaTs ($CaAlAlSiO_6$) from any $X_{Al^{VI}}$ remaining after Jd formation such that $X_{CaTs} = X_{Al^{VI}} - X_{Jd}$
9. Form CaTi ($CaTiAl_2O_6$) from any Ti remaining after Np formation such that $X_{CaTi} = X_{Ti} - X_{Np}/2$; Np is only present in alkali clinopyroxenes
10. Form chomium-aluminium Tschermak's component (CrAlTs; $CaCrAlSiO_6$) from Cr such that $X_{CrAlTs} = X_{Cr}$
11. Form DiHd ($Ca(Mg,Fe^{2+},Mn)Si_2O_6$) from any Ca remaining after Es, CaTs, CaTi and CrAlTs formation such that $X_{DiHd} = X_{Ca} - X_{Es} - X_{CaTs} - X_{CaTi} - X_{CrAlTs}$
12. Form EnFs ($(Mg,Fe^{2+},Mn)_2Si_2O_6$) from any Mg, Fe^{2+} and Mn remaining after DiHd formation such that $X_{EnFs} = (X_{Mg} + X_{Fe^{2+}} + X_{Mn}) - X_{DiHd}/2$

Although this scheme offers a far from unique solution to describing clinopyroxene compositions, it does account for all relevant elements in an internally consistent way. The results of applying this scheme to our endmember and single-crystal clinopyroxene samples is shown in Figure 7 and a worked example is provided in the Supplementary Material.

Jadeite component is formed before Ae in light of experimental and thermodynamic evidence that Na is preferentially incorporated alongside Al^{VI} rather than Fe^{3+} in magmatic clinopyroxenes dominated by quadrilateral components (Sack and Ghiorso, 1994b; Blundy et al, 1995; Putirka et al, 1996; Neave et al, 2019). For example, clinopyroxene Na contents do not correlate with f_{O_2} as would be expected if Na were preferentially incorporated as Ae. Aegirine component is then formed from relatively abundant Fe^{3+} in the case of alkali clinopyroxene like our aegirine samples or relatively scarce (or absent) residual Na in the case of all our other clinopyroxene samples (Figure 7B). Even after Ae formation, considerable Na remains in the case of the aegirine samples, necessitating the formation of an additional Np component that also accounts for the non-negligible amount of Fe^{2+} present in these crystals (e.g., Ferguson, 1977). Es, the first of several Al^{IV}-bearing components, is formed next from

any remaining Fe^{3+} (Figure 7C); Fe^{3+} is usually present in excess over Na in clinopyroxene crystals dominated by quadrilateral components. Our reasons for favouring Fe^{3+} incorporation into Es are threefold: firstly, Es is thought to be a major reservoir of Fe^{3+} in mantle clinopyroxene despite mantle crystals having higher Na:Fe^{3+} than many magmatic crystals (Luth and Canil, 1993; Blundy et al, 1995; Stolper et al, 2020); secondly, sufficient Al^{IV} is generally present alongside Si in magmatic clinopyroxene crystals to completely fill T sites without needing to incorporate tetrahedral Fe^{3+} (Morimoto et al, 1988), though some tetrahedral Fe^{3+} may occur in clinopyroxene crystals from the mantle (McGuire et al, 1991); and finally, there is tentative evidence that Fe^{3+} correlates with Ca in crystallisation experiments performed under variable f_{O_2} conditions but similar temperature conditions (Neave et al, 2019).

In line with Putirka et al (1996), CaTs is formed from any Al^{VI} remaining after Jd formation, though we note that CaTs is absent from our endmember clinopyroxene samples and occurs only in our augite samples (Figure 7D). In contrast with Putirka et al (1996), CaTi is then formed from Ti instead of Al^{IV} (Figure 7E). We do this because the approach of Putirka et al (1996) can overestimate the abundance of CaTi by ignoring other Al^{IV}-bearing components (i.e., Es and CrAlTs), and thus can imply that more Ti is incorporated into clinopyroxene crystals than actually measured by EPMA. Nonetheless, the behaviour of Ti may be more complicated than captured by our proposed scheme. For example, Ti may be balanced by minor Cr or Fe^{3+} on T sites (Morimoto et al, 1988), potentially via the fictive buffonite component (Bf; $CaMg_{0.5}Ti_{0.5}Fe^{3+}SiO_6$) of Sack and Ghiorso (1994b). It may also manifest as ABf, a generalised $NaR^{2+}_{0.5}Ti_{0.5}Si_2O_6$ component or even Ti-diopside component ($CaMgTi_2O_6$).

In contrast with Putirka et al (2003) who incorporate Cr via CrCaTs with Cr on both M1 and T sites, we incorporate Cr via chromium-aluminium Tschermak's component (CrAlTs; $CaCrAlSiO_6$). This restriction of Cr to the M1 site agrees with Cr distributions in synthetic clinopyroxenes and conventions about reporting chrome diopside compositions (Robinson, 1980; Akasaka et al, 2019). Both augite crystals and the other clinopyroxene contain variable but meaningful amounts of Cr (Figure 7F).

Diopside-hedenbergite component is formed from any Ca remaining after the formation of non-quadrilateral components. Encouragingly, our diopside and hedenbergite samples fall very close to pure DiHd component, as does the other clinopyroxene. As anticipated, our augite samples are also rich in DiHd, while our aegirine samples are almost devoid of DiHd (Figure 7G). Finally, EnFs is formed from any Mg, Fe^{2+} and Mn remaining after DiHd formation, and occurs at low but non-negligible levels across all endmember and single-crystal clinopyroxene samples (Figure 7H). Note that we group Mn and Fe^{2+} to avoid introducing additional Mn-bearing components. Our new scheme returns component sums within 0.01 of 1, indicating that all elements are suitably accounted for. Furthermore, the sums of Al^{IV}-bearing components formed from other elements or Al^{VI} (i.e., $X_{Es} + X_{CaTs} + X_{CaTi} + X_{CrAlTs}$) are within 0.001 of $X_{Al^{IV}}$ calculated from $2 - X_{Si}$.

6 Conclusions

Integrating optimised EPMA analyses of endmember and single-crystal clinopyroxene samples with Mössbauer spectroscopy reveals that clinopyroxene $Fe^{3+}/\Sigma Fe$ contents can be determined with high accuracy and precision ($1\sigma \sim 3.5\%$ absolute) using established stoichiometric approaches described by Droop (1987). This contrasts with literature opinion (McGuire et al, 1989; Canil and O'Neill, 1996). However, this apparent conflict likely reflects the optimisation of analytical methods to otanin good counting statistics across all major and minor elements as well as the better performance of the Droop (1987) approach when applied to magmatic clinopyroxene with respect to the popular Papike (1974) approach. Nevertheless, further work is required to evaluate the suitability of using currently available clinopyroxene standards to validate the accuracy of EPMA data used for determining clinopyroxene $Fe^{3+}/\Sigma Fe$.

Being able to routinely estimate clinopyroxene $Fe^{3+}/\Sigma Fe$ contents to a geologically useful level of precision, especially when averaging over large numbers of analyses, allows us to devise an empirical scheme for assigning clinopyroxene components that explicitly accounts for their Fe^{3+} contents. By integrating published observations from natural and experimental systems with our analyses, we propose that most Fe^{3+} is incorporated as Es; substantial amounts of Fe^{3+} are only present in Ae in alkali-rich pyroxenes. By changing how Ti and Cr are assigned to Al^{IV}-bearing components we also improve previous schemes by correctly balancing Al^{IV} and Al^{VI} against the other cations present. We emphasise, however, that the the outputs of our scheme cannot be used in place of those from prior schemes used for clinopyroxene thermobarometry (e.g., Putirka, 2008). That is, when applying thermobarometric models, it is essential to calculate clinopyroxene components in exactly the same way as during model calibrations or the model outputs will be invalid. We nonetheless hope that our revised approach to clinopyroxene componentry offers a framework for providing more complete descriptions of clinopyroxene compositions in future, even if this requires new analyses in the case of many legacy datasets.

Acknowledgements

We thank Lee Paul, David Olivier and Lewis Hughes at the University of Manchester for their help with sample preparation, thin section cutting and scanning electron microscopy, respectively. We also thank Stuart Kearns and Ben Buse for their help with EPMA at the University of Bristol. Mandy Edwards and David Gelsthorpe facilitated access to collections at the University of Manchester and Manchester Museum, respectively. Olivier Namur provided valuable feedback on an earlier version of the manuscript. We note that Rudra et al (2021) and Rudra and Hirschmann (2022) had presented highly relevant clinopyroxene $Fe^{3+}/\Sigma Fe$ determinations by Fe-XANES at the time of submission. However, these two manuscripts have since been retracted and can no longer form part of our discussion. We thank Luca Caricchi and Elizabeth Cottrell for their constructive reviews and Othmar Müntener for his editorial handling. A 1" epoxy mount containing chips of the seven clinopyroxene samples is available for loan from the corresponding author on request. This work was supported by a NERC

Independent Research Fellowship (NE/T011106/1) and Royal Society Research Grant (RGS\R1\201344).

References

Akasaka M, Takasu Y, Handa M, et al (2019) Distribution of Cr^{3+} between octahedral and tetrahedral sites in synthetic blue and green $(CaMgSi_2O_6)_{95}(CaCrAlSiO_6)_5$ diopsides. Mineralogical Magazine 83(4):497–505. https://doi.org/10.1180/mgm.2019.1

Batanova VG, Sobolev AV, Thomson J, et al (2017) Preliminary Data on new Olivine reference material MongOL Sh11-2 for in-situ microanalysis. In: Goldschmidt Conference Abstracts 2017, p 2822

Blundy JD, Falloon TJ, Wood BJ, et al (1995) Sodium partitioning between clinopyroxene and silicate melts. Journal of Geophysical Research: Solid Earth 100(B8):15501–15515

Brounce M, Stolper E, Eiler J (2017) Redox variations in Mauna Kea lavas, the oxygen fugacity of the Hawaiian plume, and the role of volcanic gases in Earth's oxygenation. Proceedings of the National Academy of Sciences 114(34):8997–9002. https://doi.org/10.1073/pnas.1619527114

Bryan WB, Thompson G, Ludden JN (1981) Compositional variation in normal MORB from 22°–25°N: Mid-Atlantic Ridge and Kane Fracture Zone. Journal of Geophysical Research 86(B12):11815–11836. https://doi.org/10.1029/JB086iB12p11815

Canil D, O'Neill HSC (1996) Distribution of Ferric Iron in some Upper-Mantle Assemblages. Journal of Petrology 37(3):609–635. https://doi.org/10.1093/petrology/37.3.609

Deer W, Howie RA, Zussman J (2013) An introduction to the rock-forming minerals. Mineralogical Society, London

Droop GTR (1987) A general equation for Estimating Fe^{3+} concentrations in ferromagnesian silicates and oxides from microprobe analyses, using stoichiometric criteria. Mineralogical Magazine 51(361):431–435. https://doi.org/10.1180/minmag.1987.051.361.10

Dyar MD, Gunter ME, Delany JS, et al (2002) Systematics in the structure and XANES spectra of pyroxenes, amphiboles, and micas as derived from oriented single crystals. Canadian Mineralogist 40(5):1375–1393. https://doi.org/10.2113/gscanmin.40.5.1375

Ferguson AK (1977) The Natural Occurrence of Aegirine-Neptunite Solid Solution. Contributions to Mineralogy and Petrology 253:247–253

Fournelle J, Scott J (2017) Minerals from the Kakanui Volcanic Breccia: A 2017 Look at Geological Reference Materials for EPMA. Microscopy and Microanalysis 23(S1):502–503. https://doi.org/10.1017/S1431927617003191

Frost BR (1991) Introduction to oxygen fugacity and its petrologic importance. Reviews in Mineralogy and Geochemistry 25:1–9

Ghiorso MS, Sack RO (1995) Chemical mass transfer in magmatic processes IV. A revised and internally consistent thermodynamic model for the interpolation and extrapolation of liquid-solid equilibria in magmatic systems at elevated temperatures and pressures. Contributions to Mineralogy and Petrology 119(2-3):197–212. https://doi.org/10.1007/BF00307281

Green E, Holland T, Powell R (2007) An order-disorder model for omphacitic pyroxenes in the system jadeite-diopside-hedenbergite-acmite, with applications to eclogitic rocks. American Mineralogist 92(7):1181–1189. https://doi.org/10.2138/am.2007.2401

Hammer JE, Jacob S, Welsch B, et al (2016) Clinopyroxene in postshield Haleakala ankaramite 1. Efficacy of thermobarometry. Contributions to Mineralogy and Petrology 171:7. https://doi.org/10.1007/s00410-015-1212-x

Höfer HE, Brey GP (2007) The iron oxidation state of garnet by electron microprobe: Its determination with the flank method combined with major-element analysis. American Mineralogist 92(5-6):873–885. https://doi.org/10.2138/am.2007.2390

Höfer HE, Brey GP, Schulz-Dobrick B, et al (1994) The determination of the oxidation state of iron by the electron microprobe. European Journal of Mineralogy 6(3):407–418. https://doi.org/10.1127/ejm/6/3/0407

Holland TJB, Powell R (1998) An internally consistent thermodynamic data set for phases of petrological interest. Journal of Metamorphic Geology 16(3):309–343. https://doi.org/10.1111/j.1525-1314.1998.00140.x

Holland TJB, Green ECR, Powell R (2018) Melting of peridotites through to granites: a simple thermodynamic model in the system KNCFMASHTOCr. Journal of Petrology 59(5):881–900. https://doi.org/10.1093/petrology/egy048

Jakobsson SP, Jónsson J, Shido F (1978) Petrology of the western Reykjanes Peninsula, Iceland. Journal of Petrology 19(4):669–705. https://doi.org/10.1093/petrology/19.4.669

Jarosewich E, Gooley R, Husler J (1987) Chromium Augite - A New Microprobe Reference Sample. Geostandards and Geoanalytical Research 11(2):197–198. https://doi.org/10.1111/j.1751-908X.1987.tb00027.x

Jennings ES, Holland TJB (2015) A simple thermodynamic model for melting of peridotite in the system NCFMASOCr. Journal of Petrology pp 1–24. https://doi.org/10.1093/petrology/egv020

Klügel A, Hansteen TH, Galipp K (2005) Magma storage and underplating beneath Cumbre Vieja volcano, La Palma (Canary Islands). Earth and Planetary Science Letters 236(1-2):211–226. https://doi.org/10.1016/j.epsl.2005.04.006

Larsen LM (1976) Clinopyroxenes and Coexisting Mafic Minerals from the Alkaline Ilimaussaq Intrusion, South Greenland. Journal of Petrology 17(2):258–290. https://doi.org/10.1093/petrology/17.2.258

Leung IS (1974) Sector-zoned Titanaugites: Morphology, Crystal Chemistry, and Growth. American Mineralogist 59:127–138

Lindsley DH (1983) Pyroxene thermometry. American Mineralogist 68(5-6):477–493. https://doi.org/10.1007/BF00372872

Luth RW, Canil D (1993) Ferric iron in mantle-derived pyroxenes and a new oxybarometer for the mantle. Contributions to Mineralogy and Petrology 113(2):236–248. https://doi.org/10.1007/BF00283231

Maclennan J, McKenzie D, Grönvold K, et al (2003) Melt mixing and crystallization under Theistareykir, northeast Iceland. Geochemistry, Geophysics, Geosystems 4(11):1–40. https://doi.org/10.1029/2003GC000558

McCammon C (2021) Mössbauer Spectroscopy with High Spatial Resolution: Spotlight on Geoscience. In: Yoshida Y, Langouche G (eds) Modern Mössbauer Spectroscopy, vol 137. Springer Singapore, Singapore, p 221–266, https://doi.org/10.1007/978-981-15-9422-9_5

McCammon CA (1994) A Mössbauer milliprobe: Practical considerations. Hyperfine Interactions 92:1235–1239. https://doi.org/doi.org/10.1007/BF02065761

McCanta MC, Dyar MD, Rutherford MJ, et al (2004) Iron partitioning between basaltic melts and clinopyroxene as a function of oxygen fugacity. American Mineralogist 89(11-12):1685–1693. https://doi.org/10.2138/am-2004-11-1214, iSBN: 0003-004X

McGuire AV, Dyar MD, Ward KA (1989) Neglected Fe^{3+}/Fe^{2+} ratios – a study of Fe^{3+} content of megacrysts from alkali basalts. Geology 17(8):687–690. https://doi.org/10.1130/0091-7613(1989)017<0687:NFFRAS>2.3.CO

McGuire AV, Dyar MD, Nielson JE (1991) Metasomatic oxidation of upper mantle periodotite. Contributions to Mineralogy and Petrology 109(2):252–264. https://doi.org/10.1007/BF00306483, URL http://link.springer.com/10.1007/BF00306483

Mollo S, Del Gaudio P, Ventura G, et al (2010) Dependence of clinopyroxene composition on cooling rate in basaltic magmas: Implications for thermobarometry. Lithos 118(3-4):302–312. https://doi.org/10.1016/j.lithos.2010.05.006

Mollo S, Putirka KD, Misiti V, et al (2013) A new test for equilibrium based on clinopyroxene-melt pairs: Clues on the solidification temperatures of Etnean alkaline melts at post-eruptive conditions. Chemical Geology 352:92–100. https://doi.org/10.1016/j.chemgeo.2013.05.026

Morimoto N, Fabries J, Ferguson AK, et al (1988) Nomenclature of pyroxenes. American Mineralogist 73:1123–1133. https://doi.org/10.1007/BF01226262

Moussallam Y, Edmonds M, Scaillet B, et al (2016) The impact of degassing on the oxidation state of basaltic magmas: A case study of Kīlauea volcano. Earth and Planetary Science Letters 450:317–325. https://doi.org/10.1016/j.epsl.2016.06.031

Moussallam Y, Longpré MA, McCammon CA, et al (2019) Mantle plumes are oxidised. Earth and Planetary Science Letters 527:115798. https://doi.org/10.1016/j.epsl.2019.115798

Neave DA, Putirka KD (2017) A new clinopyroxene-liquid barometer, and implications for magma storage pressures under Icelandic rift zones. American Mineralogist 102:777–794. https://doi.org/10.2138/am-2017-5968

Neave DA, Bali E, Guðfinnsson GH, et al (2019) Clinopyroxene–liquid equilibria and geothermobarometry in natural and experimental tholeiites: the 2014–2015 Holuhraun eruption, Iceland. Journal of Petrology 60:1653–1680. https://doi.org/10.1093/petrology/egz042

Papike JJ (1974) Amphiboles and pyroxenes : Characterization of other than quadrilateral components estimates of ferric iron from microprobe data. Geological Society of America Abstract with Programs 6:1053–1054

Petrone CM, Bugatti G, Braschi E, et al (2016) Pre-eruptive magmatic processes re-timed using a non-isothermal approach to magma chamber dynamics. Nature Communications 7:12946. https://doi.org/10.1038/ncomms12946

Powell R, Holland TJB, Worley N (1998) Calculating phase diagrams involving solid solutions via non-linear equations, with examples using THERMOCALC. Journal of Metamorphic Geology 16:577–588. https://doi.org/10.1111/j.1525-1314.1998.00157.x

Prescher C, McCammon C, Dubrovinsky L (2012) *MossA*: a program for analyzing energy-domain Mössbauer spectra from conventional and synchrotron sources. Journal of Applied Crystallography 45(2):329–331. https://doi.org/10.1107/S0021889812004979

Putirka KD (2008) Thermometers and Barometers for Volcanic Systems. Reviews in Mineralogy and Geochemistry 69(1):61–120. https://doi.org/10.2138/rmg.2008.69.3

Putirka KD, Johnson M, Kinzler RJ, et al (1996) Thermobarometry of mafic igneous rocks based on clinopyroxene-liquid equilibria, 0–30 kbar. Contributions to Mineralogy and Petrology 123(1):92–108. https://doi.org/10.1007/s004100050145

Putirka KD, Mikaelian H, Ryerson F, et al (2003) New clinopyroxene-liquid thermobarometers for mafic, evolved, and volatile-bearing lava compositions, with applications to lavas from Tibet and the Snake River Plain, Idaho. American Mineralogist 88(10):1542–1554. https://doi.org/10.2138/am.2005.431

Reay A, Johnstone R, Kawachi Y (1989) Kaersutite, a possible international microprobe standard. Geostandards and Geoanalytical Research 13(1):187–190. https://doi.org/10.1111/j.1751-908X.1989.tb00471.x

Robinson P (1980) The composition space of terrestrial pyroxenes -internal and external limits. Reviews in Mineralogy and Geochemistry 7:419–494. https://doi.org/10.1515/9781501508257-013

Rudra A, Hirschmann MM (2022) Fe3+ partitioning between clinopyroxene and silicate melt at 1-2.5 GPa: implications for Fe3+ content of MORB and OIB source mantle. Geochimica et Cosmochimica Acta 328:258–279. https://doi.org/10.1016/j.gca.2022.04.023

Rudra A, Cottrell E, Hirschmann MM (2021) Experimental determination of ferric iron partitioning between pyroxene and melt at 100 kPa. Chemical Geology 584:120532. https://doi.org/10.1016/j.chemgeo.2021.120532

Sack RO, Carmichael ISE (1984) Fe_2-Mg_2 and $TiAl_2$-$MgSi_2$ exchange reactions between clinopyroxenes and silicate melts. Contributions to Mineralogy and Petrology 85(2):103–115. https://doi.org/10.1007/BF00371701

Sack RO, Ghiorso MS (1994a) Thermodynamics of multicomponent pyroxenes: I. Formulation of a general model. Contributions to Mineralogy and Petrology 116(3):277–286. https://doi.org/10.1007/BF00306497

Sack RO, Ghiorso MS (1994b) Thermodynamics of multicomponent pyroxenes: III. Calibration of $Fe^{2+}(Mg)_{-1}$, $TiAl_2(MgSi_2)_{-1}$, $TiFe^{3+}{}_2(MgSi_2)_{-1}$, $AlFe^{3+}(MgSi)_{-1}$, $NaAl(CaMg)_{-1}$, $Al_2(MgSi)_{-1}$ and $Ca(Mg)_{-1}$ exchange reactions between pyroxenes and silicate melts. Contributions to Mineralogy and Petrology 118(3):271–296. https://doi.org/10.1007/BF00306648

Shorttle O, Moussallam Y, Hartley ME, et al (2015) Fe-XANES analyses of Reykjanes Ridge basalts: Implications for oceanic crust's role in the solid Earth oxygen cycle. Earth and Planetary Science Letters 427:272–285. https://doi.org/10.1016/j.epsl.2015.07.017

Smith DGW, O'Nions RK (1971) Investigations of the LII, III X-ray emission spectra of Fe by the electron microprobe Part I: Some aspects of the Fe LII, III spectra from metallic iron and haematite. Journal of Physics D: Applied Physics 4(1):147–159. https://doi.org/10.1088/0022-3727/4/1/320

Sobolev VN, Mccammon CA, Taylor LA, et al (1999) Precise Mössbauer milliprobe determination of ferric iron in rock-forming minerals and limitations of electron microprobe analysis. American Mineralogist 84:78–85

Steven CJ, Dyar MD, McCanta M, et al (2022) The absorption indicatrix as an empirical model to describe anisotropy in X-ray absorption spectra of pyroxenes. American Mineralogist 107(4):654–663. https://doi.org/10.2138/am-2021-7950

Stolper EM, Shorttle O, Antoshechkina PM, et al (2020) The effects of solid-solid phase equilibria on the oxygen fugacity of the upper mantle. American Mineralogist https://doi.org/10.2138/am-2020-7162

Ubide T, Kamber BS (2018) Volcanic crystals as time capsules of eruption history. Nature Communications 9(1):326. https://doi.org/10.1038/s41467-017-02274-w

Ubide T, Mollo S, Zhao JX, et al (2019) Sector-zoned clinopyroxene as a recorder of magma history, eruption triggers, and ascent rates. Geochimica et Cosmochimica Acta 251:265–283. https://doi.org/10.1016/j.gca.2019.02.021

Wang X, Hou T, Wang M, et al (2021) A new clinopyroxene thermobarometer for mafic to intermediate magmatic systems. European Journal of Mineralogy 33(5):621–637. https://doi.org/10.5194/ejm-33-621-2021

Weis FA, Skogby H, Troll VR, et al (2015) Magmatic water contents determined through clinopyroxene: Examples from the Western Canary Islands, Spain. Geochemistry, Geophysics, Geosystems 16:2127–2146. https://doi.org/10.1002/2015GC005800

White JC, Ren M, Parker DF (2005) Variation in mineralogy, temperature, and oxygen fugacity in a suite of strongly peralkaline lavas and tuffs, Pantelleria, Italy. Canadian Mineralogist 43(4):1331–1347. https://doi.org/10.2113/gscanmin.43.4.1331

Wieser PE, Kent AJR, Till CB, et al (2023) Barometers Behaving Badly I: Assessing the Influence of Analytical and Experimental Uncertainty on Clinopyroxene Thermobarometry Calculations at Crustal Conditions. Journal of Petrology 64(2):1–27. https://doi.org/10.1093/petrology/egac126

Wood BJ, Blundy JD (1997) A predictive model for rare earth element partitioning between clinopyroxene and anhydrous silicate melt. Contributions to Mineralogy and Petrology 129(2-3):166–181. https://doi.org/10.1007/s004100050330

Zhang HL, Cottrell E, Solheid PA, et al (2018) Determination of Fe^{3+}/Fe of XANES basaltic glass standards by Mössbauer spectroscopy and its application to the oxidation state of iron in MORB. Chemical Geology 479:166–175. https://doi.org/10.1016/j.chemgeo.2018.01.006

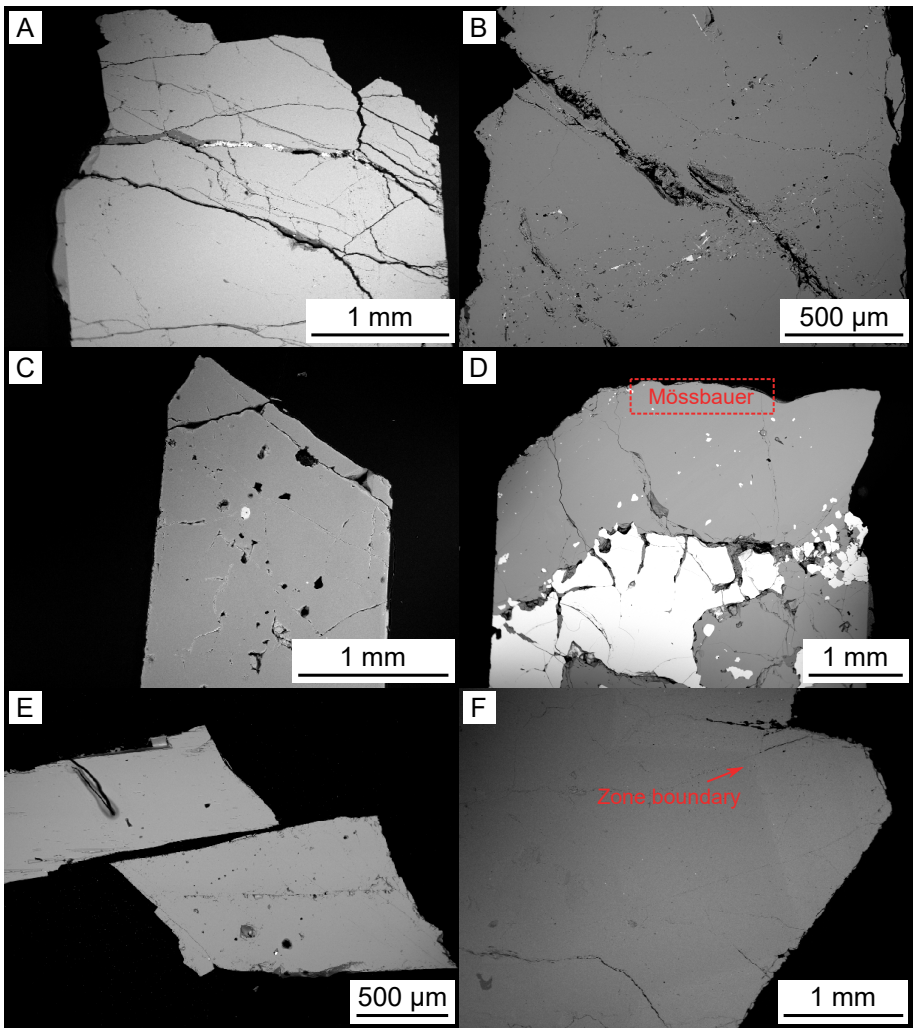

Fig. 1: Backscattered electron (BSE) images of endmember and single-crystal clinopyroxene samples. (A) Aegirine 1 shows no evidence for compositional zoning; some fractures contain low volumes of low- and high-BSE-intensity phases. (B) Aegirine 2 shows no evidence for compositional zoning but contains some diffuse bands defined by small crystals of high BSE intensity. (C) Most pieces of augite 1 show no evidence for compositional zoning, but does contain occasional high-BSE-intensity crystals of Fe-Ti oxide as identified from energy dispersive X-ray spectroscopy (EDS). (D) Augite 2 appears compositionally homogeneous but contains abundant high-BSE-intensity inclusions of Fe-Ti oxide. M aterial for Mössbauer spectroscopy was mechanically sampled from the inclusion-free portion of the crystal labelled with 'Mössbauer'. (E) The diopside shows no evidence of compositional zoning. (F) The other clinopyroxene is free of inclusions but shows clear compositional zoning as highlighted with the arrow.

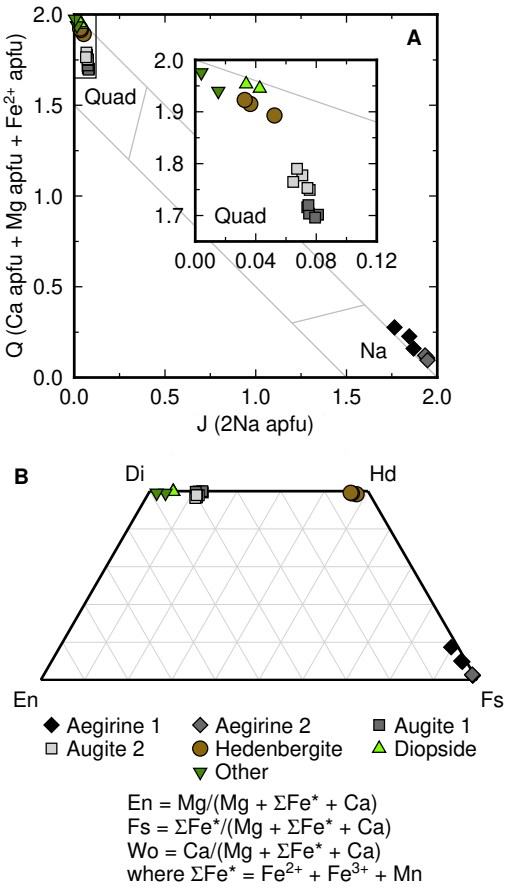

Fig. 2: Classification of endmember and single-crystal clinopyroxene samples according to Morimoto et al (1988). (A) Q–J diagram calcaulted using element abundances as atoms per formula unit (apfu). All clinopyroxene crystals considered are dominated by quadrilateral (Quad) components with the exception of Aegirine 1 and 2. (B) Pyroxene quadrilateral calculated after Morimoto et al (1988) with endmember calculations performed with the Fe component (ΣFe*) equal to the sum of Fe^{2+}, Fe^{3+} and Mn although Fe^{3+} is not accommodated within quadrilateral components (diopside, Di; hedenbergite, Hd; enstatite, En; and ferrosilite, Fs). Most clinopyroxene compositions fall between Di and Hd; our diopside and hedenbergite endmembers are almost pure. Aegirine 1 and 2 fall at the ferrosilite apex, reflecting the absence of Ca-bearing components.

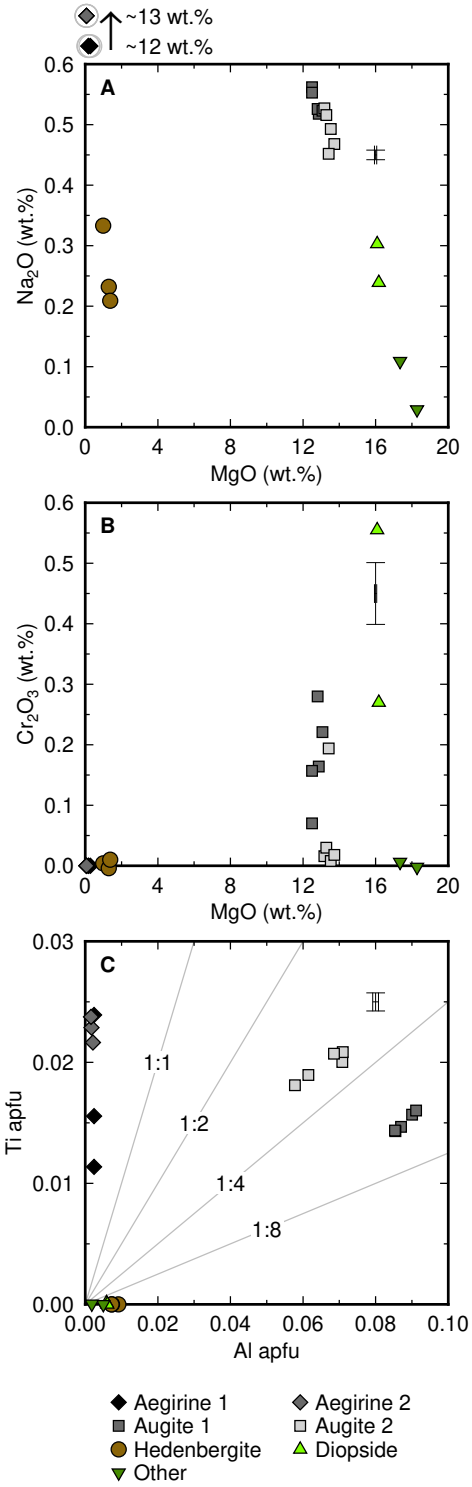

Fig. 3: Summary of key non-quadrilateral major and minor elements in endmember and single crystal clinopyroxenes; 1σ analytical uncertainties are shown. (A) Variation in Na_2O as a function of MgO. (B) Variation in Cr_2O_3 as a function of MgO. (C) Covariation of Ti and Al atoms per formula unit (apfu) calculated on six oxygen basis.

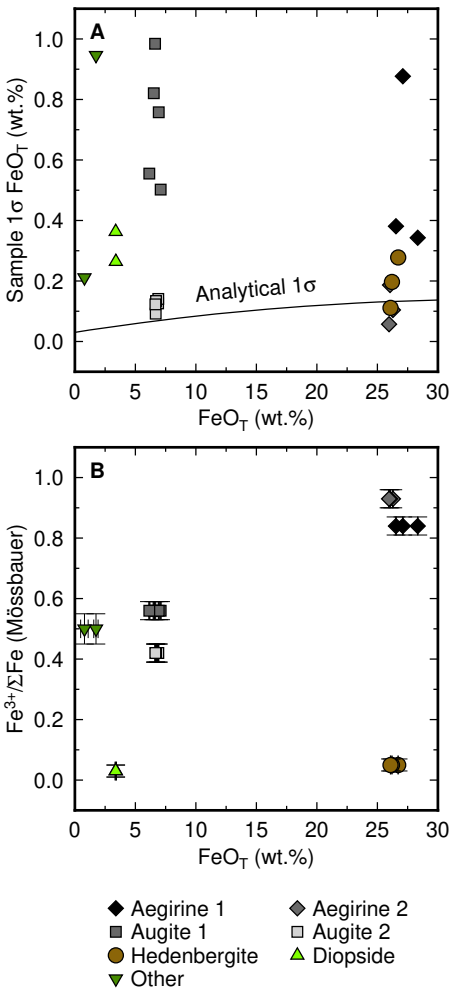

Fig. 4: Iron concentration systematics in endmember and single-crystal clinopyroxene samples. (A) Total Fe expressed as FeO (FeO_T) versus the standard deviation of FeO_T in individual pieces of endmember or single-crystal clinopyroxene samples. The concentration dependence of 1σ analytical uncertainties from EPMA counting statistics are shown as a black line. Variability in augite 2, aegirine 2 and hedenbergite is comparable with expected analytical uncertainty while variability in other clinopyroxene crystals is outwith the bounds of analytical uncertainty. (B) FeO_T versus the ratio of Fe^{3+} to total Fe ($Fe^{3+}/\Sigma Fe$, where $\Sigma Fe = Fe^{2+} + Fe^{3+}$) determined by Mössbauer spectroscopy for powdered aliquots of each clinopyroxene; 1σ analytical uncertainties are shown.

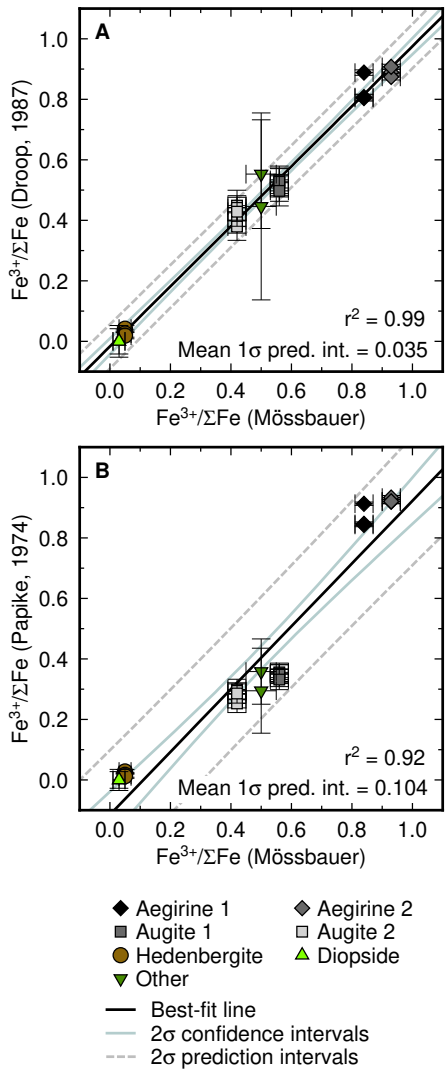

Fig. 5: Iron valence systematics in endmember and single-crystal clinopyroxene samples; 1σ uncertainties in stoichiometric determinations were estimated using a Monte-Carlo approach whereby EPMA data were repeatedly resampled according to their analytical uncertainties. (A) $Fe^{3+}/\Sigma Fe$ determined by Mössbauer spectroscopy versus $Fe^{3+}/\Sigma Fe$ determined by stoichiometry following Droop (1987). Linear regression shows that $Fe^{3+}/\Sigma Fe$ calculated following Droop (1987) can reproduce $Fe^{3+}/\Sigma Fe$ within the uncertainty of Mössbauer analyses. (B) $Fe^{3+}/\Sigma Fe$ determined by Mössbauer sectroscopy versus $Fe^{3+}/\Sigma Fe$ determined by stoichiometry following Papike (1974). Although the approach of Papike (1974) can accurately reproduce the $Fe^{3+}/\Sigma Fe$ systematics of the diopside, hedenbergite and aegirine samples, it cannot reproduce the compositions of augite samples and the other clinopyroxene that are relevant for the majority of natural magmatic clinopyroxene crystals.

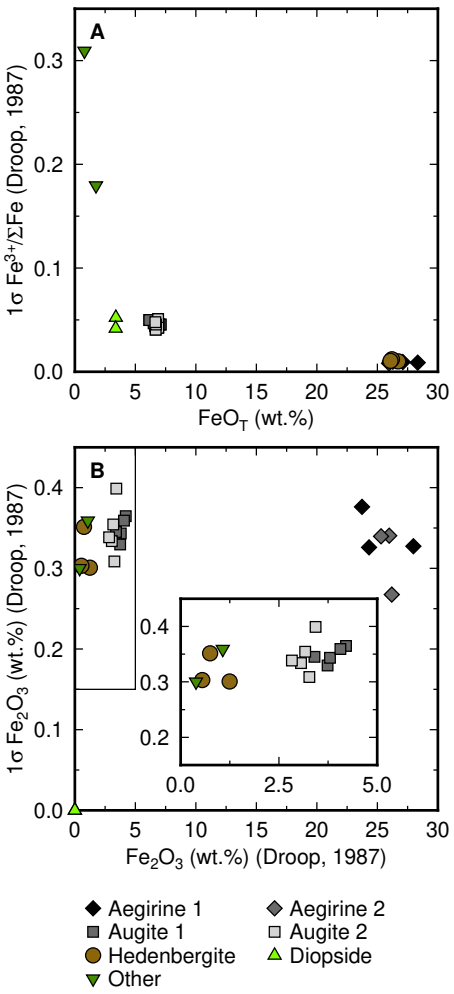

Fig. 6: Estimated uncertainties in clinopyroxene Fe valence and Fe_2O_3 content determined by stoichometry. Uncertainties in stoichiometric determinations were estimated using a Monte-Carlo approach whereby EPMA data were repeatedly resampled according to their analytical uncertainties. (A) $Fe^{3+}/\Sigma Fe$ uncertainties in endmember and single-crystal clinopyroxene samples determined following Droop (1987) and expressed at the 1σ level as a function of clinopyroxene total Fe expressed as FeO (FeO_T). (B) Fe_2O_3 uncertainties in endmember and single-crystal clinopyroxene samples determined following Droop (1987) and expressed at the 1σ level as a function of clinopyroxene Fe_2O_3 content. The inset panel expands the upper left region of the main plot.

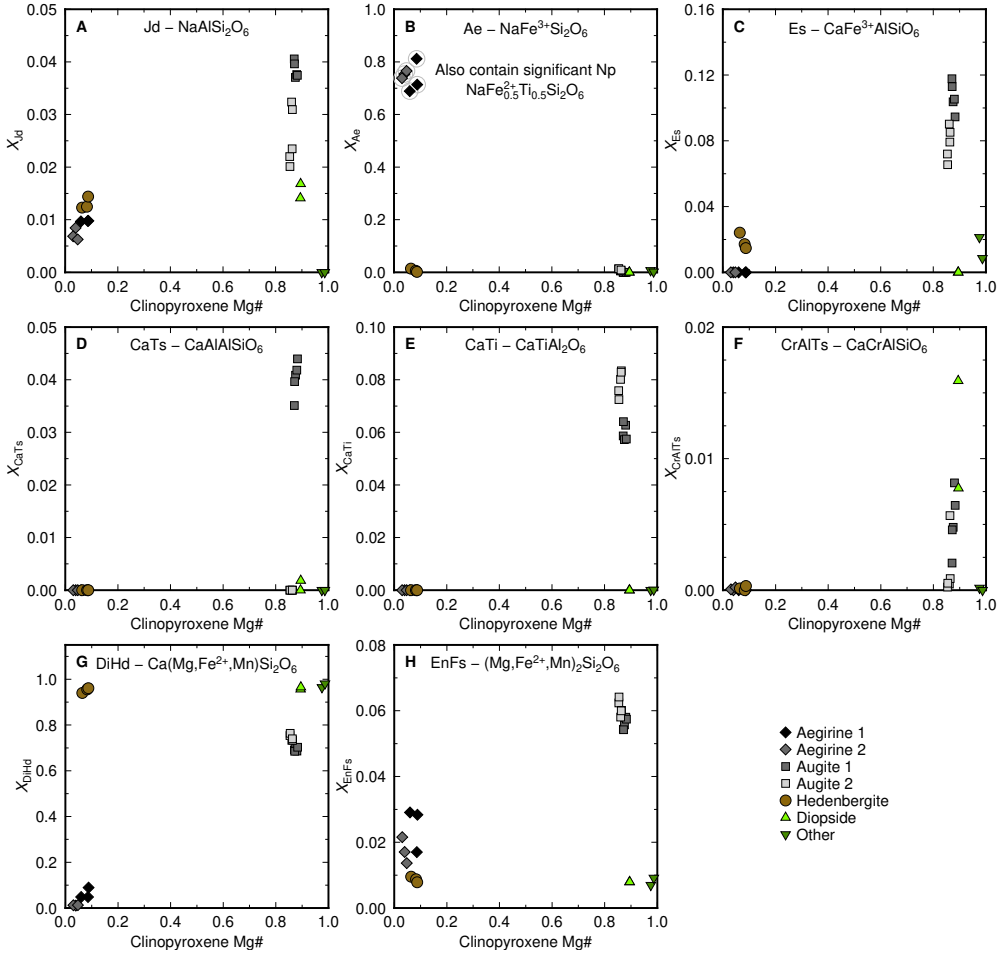

Fig. 7: Clinopyroxene components in endmember and single-crystal clinopyroxene samples. Clinopyroxene Mg# is expressed as $Mg/(Mg+Fe^{2+})$ with Fe^{2+} determined following Droop (1987). The scheme for calculating the following components is described in the main text: (A) jadeite, Jd; (B) aegirine, Ae (and neptunite, Np); (C) esseneite, Es; (D) calcium-Tschermak's component, CaTs; (E) titanium pyroxene component, CaTi; (F) chromian calcium-Tschermak's component, CrCaTs; (G) diopside and hedenbergite, DiHd; and (H) enstatite and ferrosilite, EnFs.

Table 1: Endmember and single-crystal clinopyroxene samples studied

Sample	Source	Sample ID	Locality	Sample type
Aegirine 1	DEES[a]	502	Unknown	Single crystals extracted from alkaline igneous rock containing aegirine, feldspar and quartz
Aegirine 2	MM[b]	N3027	Norway	Loose single crystals
Augite 1	DEES	746	Laacher See, Germany	Loose single crystals
Augite 2	DEES	Zn6.6	Unknown	Loose single crystals
Diopside	DEES	4020	Unknown	Large (>1 cm) intergrown crystals of metamorphic diopside
Hedenbergite	DEES	2513	Elba Island, Italy	Small (<1 mm) fibrous intergrown hedenbergite skarn
Other	DEES	499	Unknown	Moderate (∼ 5 mm) intergrown, vuggy crystals

[a]Department of Earth and Environmental Sciences at The University of Manchester, [b] Manchester Museum

Table 2: Mean major element compositions of aegirine 1, aegirine 2, augite 1 and augite 2 determined by EPMA ($\bar{x}$); Fe_2O_3 and FeO contents were determined following Droop (1987). $Fe^{3+}/\Sigma Fe$ contents from Mössbauer spectroscopy and calculated with the approaches of Droop (1987) and Papike (1974) and are also shown. 1σ uncertainties from repeat analyses ($1\sigma_r$; an indication of homogeneity) and EPMA counting statistics ($1\sigma_a$; an indication of analytical uncertainty) are shown for all elements except Fe. $1\sigma_a$ values for Fe_2O_3, FeO and $Fe^{3+}/\Sigma Fe$ from Droop (1987) and Papike (1974) were derived from the Monte Carlo approach described in the main text and $1\sigma_a$ values for Mössbauer spectroscopy were derived from MossA fitting (Prescher et al, 2012).

	Aegirine 1			Aegirine 2			Augite 1			Augite 2		
	$\bar{x}$	$1\sigma_r$	$1\sigma_a$	$\bar{x}$	$1\sigma_r$	$1\sigma_a$	$\bar{x}$	$1\sigma_r$	$1\sigma_a$	$\bar{x}$	$1\sigma_r$	$1\sigma_a$
SiO_2 (wt.%)	52.07	0.33	0.16	52.06	0.26	0.16	46.73	0.58	0.15	47.61	0.69	0.15
TiO_2	2.33	0.26	0.06	3.11	0.09	0.07	2.15	0.18	0.06	2.81	0.26	0.07
Al_2O_3	0.21	0.03	0.02	0.16	0.02	0.02	8.04	0.58	0.07	5.97	0.58	0.06
Cr_2O_3	0.00	0.01	0.01	0.00	0.01	0.00	0.17	0.18	0.04	0.04	0.03	0.02
Fe_2O_3	25.34		0.34	25.86		0.32	3.84		0.35	3.13		0.34
FeO	4.52		0.25	2.85		0.24	3.21		0.31	3.95		0.30
MnO	1.09	0.10	0.02	1.70	0.06	0.02	0.11	0.02	0.01	0.11	0.01	0.01
MgO	0.21	0.07	0.02	0.06	0.01	0.01	12.75	0.50	0.06	13.45	0.29	0.07
CaO	1.49	0.38	0.04	0.28	0.03	0.02	22.86	0.22	0.15	22.75	0.15	0.15
Na_2O	12.17	0.24	0.03	12.94	0.08	0.03	0.54	0.08	0.01	0.49	0.04	0.01
Total	99.43			99.03			100.39			100.32		
n EPMA	9			25			26			22		
$Fe^{3+}/\Sigma Fe$ Mössbauer	0.84		0.03	0.93		0.03	0.56		0.03	0.42		0.03
$Fe^{3+}/\Sigma Fe$ Droop (1987)	0.83		0.01	0.89		0.01	0.52		0.05	0.42		0.04
$Fe^{3+}/\Sigma Fe$ Papike (1974)	0.87		0.01	0.93		0.01	0.35		0.03	0.28		0.03

Table 3: Mean major element compositions of diopside, hedenbergite and the other clinopyroxene determined by EPMA ($\bar{x}$); Fe_2O_3 and FeO contents were determined following Droop (1987). $Fe^{3+}/\Sigma Fe$ contents from Mössbauer spectroscopy and calculated with the approaches of Droop (1987) and Papike (1974) and are also shown. 1σ uncertainties from repeat analyses ($1\sigma_r$; an indication of homogeneity) and EPMA counting statistics ($1\sigma_a$; an indication of analytical uncertainty) are shown for all elements except Fe. $1\sigma_a$ values for Fe_2O_3, FeO and $Fe^{3+}/\Sigma Fe$ from Droop (1987) and Papike (1974) were derived from the Monte Carlo approach described in the main text and $1\sigma_a$ values for Mössbauer spectroscopy were derived from MossA fitting (Prescher et al, 2012).

	Diopside			Hedenbergite			Other		
	$\bar{x}$	$1\sigma_r$	$1\sigma_a$	$\bar{x}$	$1\sigma_r$	$1\sigma_a$	$\bar{x}$	$1\sigma_r$	$1\sigma_a$
SiO_2 (wt.%)	54.90	0.19	0.16	48.96	0.23	0.16	55.43	0.39	0.16
TiO_2	0.01	0.03	0.01	0.00	0.03	0.01	0.00	0.02	0.01
Al_2O_3	0.56	0.13	0.02	0.65	0.11	0.03	0.31	0.10	0.02
Cr_2O_3	0.41	0.28	0.02	0.00	0.01	0.01	0.00	0.01	0.00
Fe_2O_3	0.00		0.00	0.81		0.32	0.70		0.33
FeO	3.38		0.16	25.57		0.27	0.59		0.28
MnO	0.11	0.02	0.01	0.89	0.04	0.02	0.59	0.30	0.02
MgO	16.13	0.16	0.07	1.24	0.09	0.02	17.86	0.50	0.07
CaO	25.05	0.25	0.15	22.41	0.29	0.14	25.73	0.34	0.16
Na_2O	0.27	0.09	0.01	0.25	0.06	0.01	0.07	0.04	0.01
Total	100.82			100.79			101.27		
n EPMA	12			11			12		
$Fe^{3+}/\Sigma Fe$	0.03		0.02	0.05		0.02	0.50		0.05
Mössbauer									
$Fe^{3+}/\Sigma Fe$	0.00		0.05	0.03		0.01	0.49		0.25
Droop (1987)									
$Fe^{3+}/\Sigma Fe$	0.00		0.03	0.02		0.01	0.34		0.13
Papike (1974)									